

## Simulations of Flexible Fiber Suspensions

Emilio J. Tozzi and Daniel J. Klingenberg

Department of Chemical and Biological Engineering, University of Wisconsin, Madison, WI 53706, USA

C. Tim Scott

USDA Forest Products Laboratory, Madison, WI 53706, USA

Pasi Miettinen

KCL Science and Consulting, FIN-02151 Espoo, FINLAND

### ABSTRACT

Fiber-level simulations are employed to probe the relationships between various properties and macroscopic behavior of flexible fiber suspensions. Issues addressed include flocculation, suspension rheology, and handsheet formation and testing. Results show that such simulations can be useful tools for understanding the factors that control the behavior of suspensions.

### INTRODUCTION

Understanding the behavior of flexible fiber suspensions is challenging because of the many variables that affect macroscopic properties (such as fiber length, concentration, shape, flexibility, interactions, etc.), and the difficulty of systematically varying the system variables in experimental studies. In this report, we show how fiber-level simulations can be used to systematically investigate the relationships between fiber properties and interactions, and the macroscopic properties of flexible fiber suspensions. We examine flocculation in fiber suspensions, rheological properties, and handsheet formation and mechanical testing.

### FIBER-LEVEL SIMULATIONS

Flexible fibers in suspension are modeled as neutrally-buoyant, linked, rigid bodies immersed in a Newtonian liquid. Each fiber is represented by  $N_{\text{seg}}$  rigid cylinders (length  $2\ell$ , radius  $b$ , overall fiber length  $L=2N_{\text{seg}}\ell$ ) with hemispherical end caps, connected end-to-end by ball and socket joints (Fig. 1). The motion of each fiber segment is described by Newton's equations of translational and rotational motion, in which we neglect fluid and fiber inertia. The evolution of the fiber shapes, orientations and positions in flow are simulated by numerically integrating the equations of motion subject to the forces and torques acting on each segment. These forces and torques are described briefly below. The model and simulation method are described in more detail elsewhere [1-9].

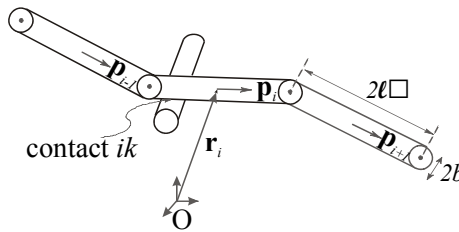


*Figure 1.* Schematic diagram of a model fiber composed of rigid spherocylinders linked by ball and socket joints. Segment  $i$  is in contact with segment  $k$  from another fiber.

Forces and torques acting on the fibers include: constraint forces that maintain the connectivity of the segments within each fiber; hydrodynamic forces and torques; bending and twisting potentials within the hinges to resist fiber deformation; short-range repulsive forces to prevent fiber overlap; and friction between fibers in contact. Hydrodynamic forces and torques are treated in the free-draining, zero Reynolds number limit. Bending and twisting torques are assumed to be linear in the deviations of the bending and twisting angles ( $\theta$  and  $\phi$ ) from their equilibrium values ( $\theta^{\text{eq}}$  and  $\phi^{\text{eq}}$ ), with bending and twisting spring constants  $k_b = E_Y I / 2\ell$  and  $k_t = E_Y J / 2\ell$  ( $E_Y$  is the

fiber Young's modulus, and  $I$  and  $J$  are the corresponding moments of inertia). For all results reported here,  $k_t = 0.67k_b$ , mimicking a linearly elastic circular cylinder with a Poisson's ratio of 0.5. The fiber stiffness is characterized by the dimensionless effective stiffness,  $S^{\text{eff}} = E_y I / \eta_0 \gamma L^4$ , where  $\eta_0$  is the suspending fluid viscosity, and  $\gamma$  is the shear rate. Friction forces are characterized by a static coefficient of friction  $\mu^{\text{stat}}$ .

## RESULTS

### Fiber Flocculation

Fiber suspensions in shear flow were simulated for a variety of parameter values. Consider first the behavior of fibers with  $N_{\text{seg}} = 5$ , aspect ratio  $r_p = L/2b = 75$ , concentration  $nL^3 = 20$ . This system can flocculate for certain ranges of the remaining parameters (fiber shape, stiffness and friction coefficient), even in absence of attractive forces, as illustrated in Fig. 2 [2,4,8]. In Fig. 2(a), the friction coefficient is large ( $\mu^{\text{stat}} = 20$ ), the fibers are stiff (effective stiffness  $S^{\text{eff}} = E_y I / \eta_0 \gamma L^4 = 0.05$ ), and the equilibrium fiber shape is not straight ( $\theta^{\text{eq}} = 0.8$  and  $\phi^{\text{eq}} = 0.7$ ). The suspension has flocculated, with two flocs apparent in the simulation box. In Figs. 2(b)-(d), one of the above features has been removed, and the suspensions remain homogeneous.

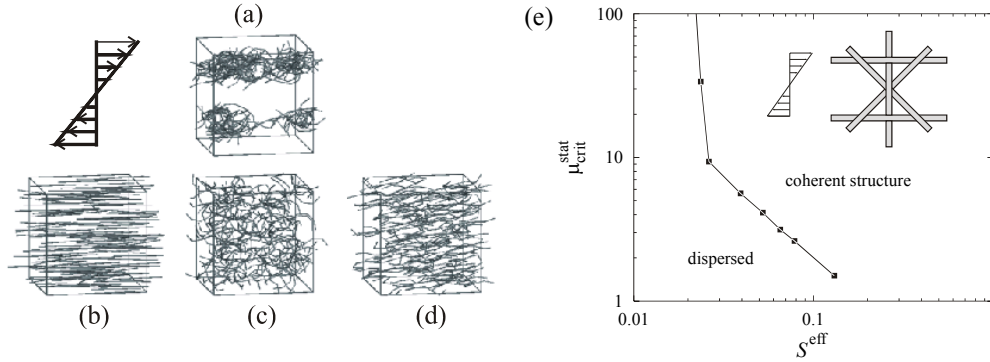


*Figure 2.* (a) Simulation snapshots after shearing to a strain of 1500, with parameters  $nL^3 = 20$ ,  $r_p = 75$ ,  $N_{\text{seg}} = 5$ , and (a)  $\mu^{\text{stat}} = 20$ ,  $S^{\text{eff}} = 0.05$ ,  $\theta^{\text{eq}} = 0.8$ ,  $\phi^{\text{eq}} = 0.7$  (flocculated suspension); (b) same as (a) except  $\theta^{\text{eq}} = \phi^{\text{eq}} = 0$ ; (c) same as (a) except  $\mu^{\text{stat}} = 0$ ; and (d) same as (a) except  $S^{\text{eff}} = 0.0005$ . (e) Critical coefficient of friction as a function of the effective stiffness for the star test floc in simple shear flow ( $N_{\text{seg}} = 7$ ,  $r_p = 56$ ,  $\theta^{\text{eq}} = 0$ ,  $\phi^{\text{eq}} = 0$ ).

Comparison of Figs. 2(a) and (d) illustrates that flocculation only occurs for fibers with sufficiently large effective stiffness, consistent with several experimental observations. Soszynski and Kerekes [10] observed that nylon fiber flocs dispersed easily when heated above the glass transition temperature to reduce elastic stresses. Several authors have also reported that flocs do not form if the suspending fluid viscosity is too large [10,11]. Since the effective stiffness  $S^{\text{eff}} \propto 1/\eta_0$ , increasing the suspending fluid viscosity is equivalent to reducing the effective stiffness, and thus the model presented here also predicts that flocs will not form for sufficiently large fluid viscosities. We note that simulations of frictionless fibers interacting via attractive forces do not exhibit this behavior [1,3], providing further support of the mechanism of friction-induced flocculation.

Although the flocculation induced by friction discussed above is consistent with experimental observations, the friction coefficient necessary to see flocculation is much larger than experimentally measured values of approximately 0.5 [12,13]. However, the dimensionless stiffnesses employed in the simulations are small compared to those typically achieved in experiments. Choosing values typical for wood fibers in water, we find that  $S^{\text{eff}}$  (expt.)  $> 1$  [1,3]. Unfortunately, simulating suspensions of fibers this stiff requires more computational power than is currently available.

To probe the behavior of suspensions composed of much stiffer fibers, we investigated the behavior of a test floc composed of five straight fibers interwoven into a “star” configuration (illustrated in the inset of Fig. 2(e);  $N_{\text{seg}} = 7$ ,  $r_p = 56$ ,  $\theta^{\text{eq}} = 0$  and  $\phi^{\text{eq}} = 0$ ). The test floc was placed in simple shear flow (in the plane of shear) and sheared to a strain of 100. For a fixed value of  $S^{\text{eff}}$ , the test floc would remain intact if  $\mu^{\text{stat}}$  were large enough, and would

disperse if  $\mu^{\text{stat}}$  were too small. The minimum value of  $\mu^{\text{stat}}$  necessary to keep the floc intact was defined as a “critical” friction coefficient,  $\mu^{\text{stat}}_{\text{crit}}$ , which is a function of  $S^{\text{eff}}$ . The critical friction coefficient is plotted as a function of  $S^{\text{eff}}$  in Fig. 2(e). As the stiffness increases, the coefficient of friction necessary to hold the floc together decreases. These results suggest that for large values of  $S^{\text{eff}}$ , comparable to those experienced experimentally ( $S^{\text{eff}} > 1$ ), the coefficient of friction necessary to see flocculation in simulations of sheared suspensions may indeed approach values measured experimentally.

### Suspension Rheology

Simulations also show that fiber properties and interactions also significantly influence the suspension rheology. The specific suspension viscosity is plotted as a function of  $1/S^{\text{eff}}$  ( $\propto \gamma$ ) for simulated suspensions with different fiber properties in Fig. 3. For suspensions of nonstraight fibers interacting with a large coefficient of friction, the viscosity increases rapidly as  $1/S^{\text{eff}}$  is decreased (A). When the coefficient of friction is reduced, the suspension viscosity decreases significantly (B). Fiber shape is also important, as straight fibers have a much smaller viscosity at the same concentration.

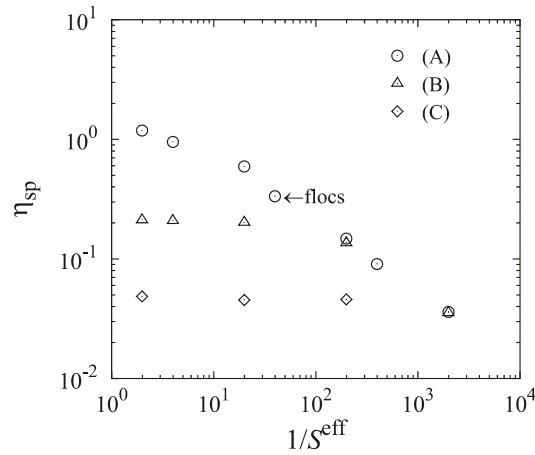


Figure 3. Specific viscosity versus the reciprocal of the effective stiffness for suspensions with concentration  $nL^3=15$  and aspect ratio  $r_p=75$  in which (A) flocculates and (B) and (C) remain homogeneous: (A)  $(\theta^{\text{eq}}, \phi^{\text{eq}}, \mu^{\text{stat}}) = (0.8, 0.7, 20)$ ; (B)  $(\theta^{\text{eq}}, \phi^{\text{eq}}, \mu^{\text{stat}}) = (0.8, 0.7, 1)$ ; (C)  $(\theta^{\text{eq}}, \phi^{\text{eq}}, \mu^{\text{stat}}) = (0.1, 0, 20)$ .

Next we investigate in more detail the effects of fiber shape and static friction on the shear viscosity of fiber suspensions. Simple shear flow was simulated for suspensions of U-shaped fibers ( $r_p = 75$ ,  $S^{\text{eff}} = 0.05$ ) at various concentrations and for several different equilibrium bending angles and coefficients of friction. U-shaped fibers with different equilibrium bending angles are illustrated in Fig. 4.

| $\theta^{\text{eq}}$ (rad.) | shape |
|-----------------------------|-------|
| 0.0                         |       |
| 0.1                         |       |
| 0.3                         |       |
| 0.6                         |       |

Figure 4. Examples of U-shaped fibers ( $\phi^{\text{eq}}=0$ ,  $r_p = 75$ ) for various values of  $\theta^{\text{eq}}$ .

The specific viscosity  $\eta_{sp} = \eta/\eta_0 - 1$  ( $\eta$  is the suspension viscosity) is plotted as a function of concentration ( $nL^3$ ) in Figs. 5(a) and (b) for suspensions of U-shaped fibers. Results are presented for simulations of flexible fibers ( $S^{\text{eff}} = 0.05$ ,  $r_p = 75$ ,  $N_{\text{seg}} = 5$ ) with  $\theta^{\text{eq}} = 0, 0.1$  and  $0.3$ , as well as for straight, rigid fibers ( $r_p = 75$ ,  $N_{\text{seg}} = 1$ ). Results for simulations without friction ( $\mu^{\text{stat}} = 0$ ) are represented by open symbols, and results for simulations with friction ( $\mu^{\text{stat}} = 20$ ) are represented by filled symbols. Figure 5(b) illustrates data over wider ranges of concentrations and specific viscosities than that presented in Fig. 5(a). The data points indicate individual simulation runs in which the average value is computed from at least 500 steady state configurations. Uncertainties (95% confidence interval) estimated from replicate simulations with different initial configurations are indicated by the error bars.

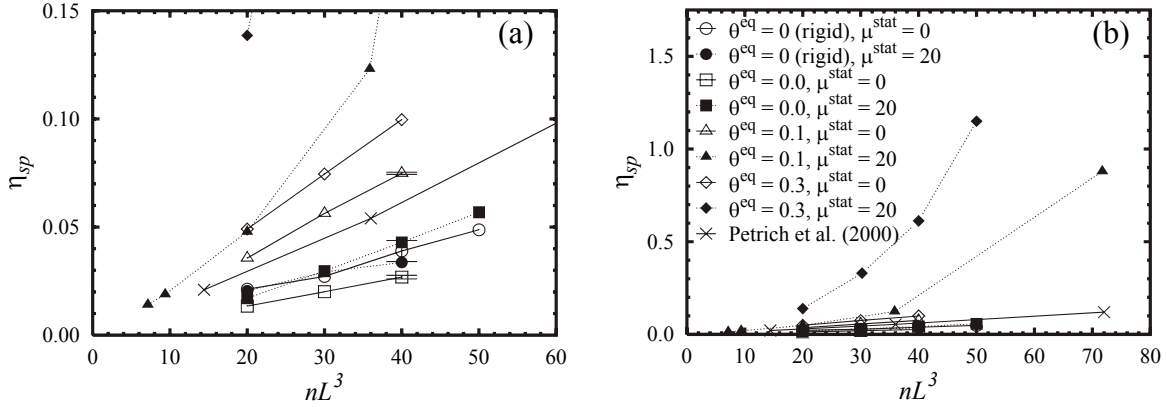


Figure 5. Steady-state specific viscosity as a function of concentration for suspensions with fibers of different shapes and coefficients of friction.

Consider first the effect of fiber flexibility in the absence of friction in these simulations, illustrated by the results for suspensions of rigid, straight fibers (open circles) and the results for suspensions of flexible, straight fibers (open squares) in Fig. 5(a). For both systems,  $\eta_{sp}$  is small, and increases roughly linearly with concentration in agreement with previous simulations at relatively small concentrations [14]. The linear dependence of the viscosity on concentration is consistent with the predictions of slender body theory for dilute fiber suspensions [15]. Petrich et al. [16] also observed this type of behavior in experiments of very stiff and straight glass fibers ( $S^{\text{eff}} \sim 1$ ) with an aspect ratio  $r_p = 72$  at approximately the same concentration range as our simulations (illustrated in Fig. 5).

The differences between the results for suspensions of straight, rigid fibers and suspensions of straight, flexible fibers are very small, approximately equal to the uncertainties. This is not unexpected, since the flexible fibers in this case are actually quite stiff. For these simulations, the average deviation of the bending angles from the equilibrium value is  $\langle |\theta_i - \theta^{\text{eq}}| \rangle = 6 \times 10^{-4}$ . Indeed, the degree of deformation for all the runs depicted in Fig. 5 is quite small, and thus the results appear to represent the behavior of stiff fibers ( $\langle |\theta_i - \theta^{\text{eq}}| \rangle = 4.6 \times 10^{-3}$  for  $\theta^{\text{eq}} = 0.1$ ;  $\langle |\theta_i - \theta^{\text{eq}}| \rangle = 1.6 \times 10^{-2}$  for  $\theta^{\text{eq}} = 0.3$ ). Effects of fiber flexibility and flocculation on suspension rheological properties are discussed elsewhere [4,6].

Next consider the effect of fiber shape in the absence of friction, illustrated by the results for straight, rigid and flexible fibers (open circles and squares, respectively), and U-shaped, flexible fibers ( $\theta^{\text{eq}} = 0.1$ , open triangles) in Fig. 5(a). The specific viscosities of the suspensions of U-shaped fibers are significantly larger than that for the suspensions of straight fibers. At  $nL^3 = 40$ ,  $\eta_{sp}$  for the U-shaped fibers is approximately twice as large as that for the straight fibers. We note that for  $\theta^{\text{eq}} = 0.1$ , the fiber shape is nearly straight (see Fig. 4). Thus a small amount of curvature can have a significant effect on the suspension viscosity.

The results presented in Fig. 5 also illustrate the impact of interfiber friction on the shear viscosity. For suspensions of straight, rigid fibers, adding static friction ( $\mu^{\text{stat}} = 20$ ) does not alter the shear viscosity. For suspensions of straight, flexible fibers, adding static friction produces a small increase in the specific viscosity. The effect of static friction is much more pronounced for the U-shaped fibers. For  $nL^3 > 30$ , adding static friction more than doubles the specific viscosity. In addition, the concentration dependence changes from a linear dependence in the absence of friction to a higher-order dependence with  $\mu^{\text{stat}} = 20$ .

To further probe the effect of fiber shape on the rheological properties of fiber suspensions, we recently developed an improved method for simulating rigid fiber dynamics in linear flows which more accurately accounts for hydrodynamic interactions between different parts of a fiber. This method is appropriate for simulating single fibers, but would be too computationally expensive for simulating concentrated fiber suspensions. The method is similar to that developed by Carrasco and de la Torre [17], and is described in more detail elsewhere [18].

This improved method was employed to simulate non-straight, rigid fibers in simple shear flow, using various aspect ratios and shapes, as illustrated in Fig. 6. The objective of this study was to determine how well various measures of fiber shape correlate with fiber suspension properties. Simulations for each fiber were performed for numerous initial conditions, and the average intrinsic viscosity was calculated. The intrinsic viscosity  $[\eta]$  is related to the suspension viscosity  $\eta$  by

$$[\eta] = \lim_{\phi \rightarrow 0} \frac{\eta / \eta_0 - 1}{\phi}, \quad (1)$$

where  $\phi$  is the fiber volume fraction.

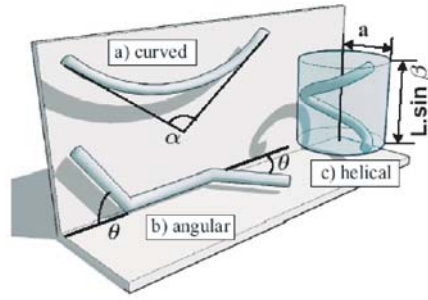


Figure 6. Fiber shapes employed in accurate simulations of dilute rigid fiber suspensions.

Previous efforts have employed various measures of fiber shape. Page [19] characterized the fiber shape by the “curl index,” which may be defined

$$\text{Curl Index} = \frac{L}{R} - 1, \quad (2)$$

where  $L$  is the fiber contour length and  $R$  is the end-to-end distance. Another measure of particle shape is the “kink index” [20], which is related to the numbers of bends of in different ranges of angles,

$$\text{Kink Index} = \frac{N_{10^\circ-20^\circ} + 2N_{21^\circ-45^\circ} + 3N_{46^\circ-90^\circ} + 4N_{91^\circ-180^\circ}}{L}, \quad (3)$$

where  $N_{\alpha_1-\alpha_2}$  is the number of bends per fiber between the angles of  $\alpha_1$  and  $\alpha_2$ . In Figure 7, the intrinsic viscosity of suspensions of variously shaped particles is plotted as a function of the curl index and the kink index, for fibers of three different overall aspect ratios. For a given aspect ratio, the intrinsic viscosity generally increases with curl index for small curl indices, but there is considerable scatter. At large values of the curl index, the intrinsic viscosity decreases with increasing curl index. Thus the rheological properties of the suspension do not correlate well with curl index, which reduces the curl index’s utility as a predictor of rheological properties. Also plotted in Fig. 7 is the intrinsic viscosity as a function of kink index. Here, there is even more scatter in the data at fixed aspect ratio, implying that rheological properties do not correlate well with kink index.

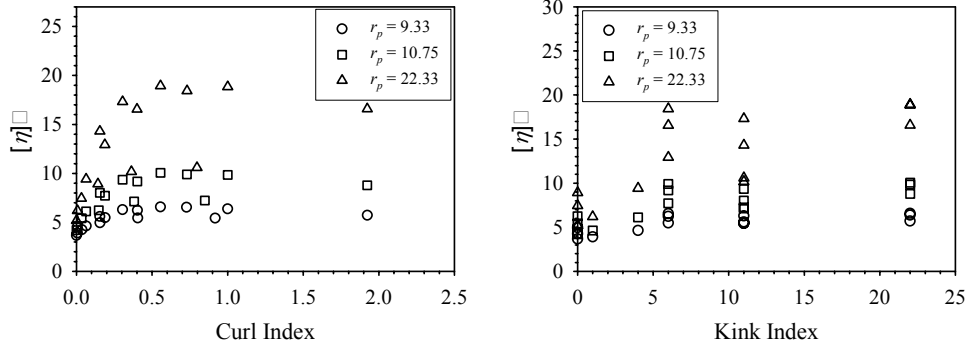


Figure 7. Intrinsic viscosity as a function of curl index and kink index for variously shaped fibers at three different aspect ratios.

We have examined a variety of other measures of particle shape [18]. Of those, we find that an invariant of the hydrodynamic translational friction tensor,

$$I_3^T = \frac{\lambda_1 \lambda_2 \lambda_3}{(\lambda_3)^3}, \quad (4)$$

where  $\lambda_1$ ,  $\lambda_2$ , and  $\lambda_3$  are the eigenvalues of the translational friction tensor ( $\lambda_3 > \lambda_2 > \lambda_1$ ), correlates well with suspension rheological properties. This is illustrated in Fig. 8 where the intrinsic viscosity for the various fiber shapes discussed above is plotted as a function of  $I_3^T$ , for three different overall aspect ratios. For each aspect ratio, the data fall roughly on a single curve, suggesting that it may be possible to accurately represent the suspension rheological properties as a simple function of  $r_p$  and  $I_3^T$ . Furthermore, the dependence on  $I_3^T$  is monotonic, particularly for larger aspect ratios, which implies that rheological properties can in principle be used to measure particle “shape” (that is, to obtain values of  $I_3^T$ ).

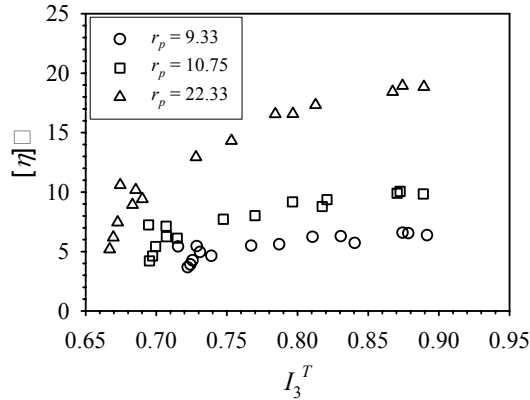
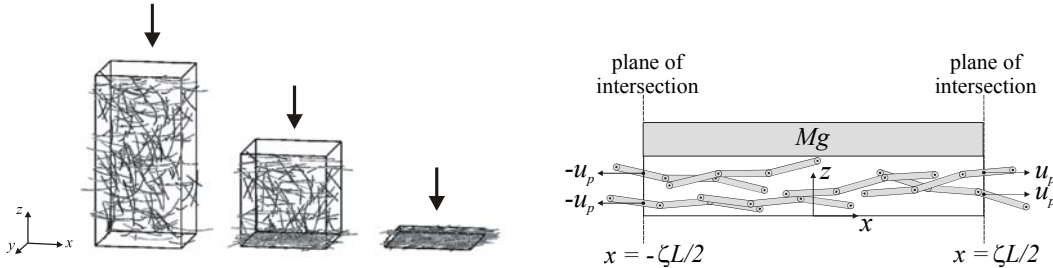


Figure 8. Intrinsic viscosity as a function of the invariant of the translational friction tensor.

One may question the utility of using  $I_3^T$  as a practical measure of particle shape, as it is in general a complicated function of the topology of the fiber. However, given the information about the shape of the fiber, for example from a microscope image,  $I_3^T$  can be calculated in a straightforward manner [18]. In fact, this is similar to the manner in which the curl or kink indices would be obtained---from measurements of the particle topology in a microscope image. Thus obtaining values for  $I_3^T$  is in principle no more complicated than obtaining values for other shape measures.

## Handsheet Formation and Mechanical Testing

Finally, we examine handsheet formation and mechanical testing via simulations [5]. Planar network formation is simulated by randomly placing fibers in a simulation cell with  $xy$  dimensions  $\zeta L \times \zeta L$  ( $\zeta = 2$  for all results reported here), and height  $2\zeta L$  in the  $z$ -direction. A solid piston of mass  $M$  is initially located at the top ( $z = 2\zeta L$ ), a semipermeable screen is located at the bottom ( $z = 0$ ), and periodic boundary conditions are applied in the  $x$  and  $y$  directions. The equations of motion for the fibers and the piston are solved numerically as the falling piston forces the suspending fluid through the screen, forming a sheet-like, three-dimensional network of entangled fibers, as illustrated in Fig. 9. The piston mass is chosen such that the final volume fraction of the network is  $\phi = 0.05 \pm 0.005$ . For the results presented, the “sheets” formed were approximately 10-15 fiber diameters in thickness, with periodic in-plane dimensions of  $2L \times 2L$ . We acknowledge that this method differs significantly from typical handsheet formation; it is employed here simply as a means for obtaining planar networks.



*Figure 9.* Illustration of sheet formation in simulations. The piston (not shown) pushes down from the top. Also shown is a schematic diagram of how mechanical testing is simulated (periodic images are not shown).

Simulation of network elongation is performed by first identifying the fiber segments that intersect the planes located at  $x = \pm\zeta L/2$  (Fig. 9). The points of intersection of these segments and the planes are constrained to move at speed  $\pm u_p$ ; the motion of the remaining segments is determined by numerical integration of their equations of motion (with the piston fixed). Periodic boundaries are maintained in the  $x$  and  $y$  directions. Short-range repulsive forces are applied at the piston and semipermeable screen surfaces. The tensile force  $T$  is evaluated as the sum of the forces required to displace the segments that intersect each plane at  $x = \pm\zeta L/2$ , averaged over the two planes. The fiber stiffness is characterized by a dimensionless effective stiffness,  $S^{\text{eff}} = E_\gamma I / \eta_0 \gamma L^4$ , where  $\gamma = u_p / b$  is a characteristic deformation rate.

In the simulation of network elongation, the piston is maintained at its final position from the formation process, in contact with the network. The resulting forces on the network (in addition to interfiber friction forces) help maintain some degree of consolidation, much like surface tension on a completely saturated network. In principle, one could also model the effect of surface tension forces caused by menisci between fibers in contact to investigate effects of water content on the network behavior [21].

Figure 10 illustrates snapshots of structures from a typical simulation at three different strains  $\varepsilon = \Delta x / \zeta L$ , for a suspension of straight, flexible fibers [ $(S^{\text{eff}}, r_p, \theta^{\text{eq}}, \phi^{\text{eq}}, \mu^{\text{stat}}) = (0.05, 75, 0, 0, 20)$ ]. The mechanical responses for these and other conditions are described below.

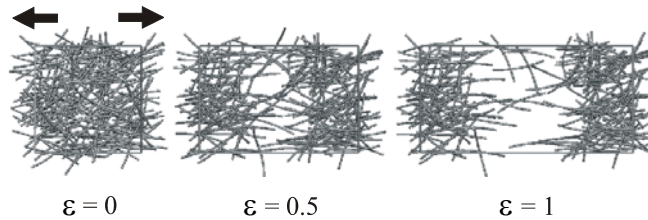


*Figure 10.* Snapshots of the structure of a typical simulated fiber network subjected to elongation at various deformations.

Fiber networks were formed using straight and U-shaped fibers ( $\theta^{\text{eq}} = 0.1$  and  $0.5$ ), in which the remaining parameters were held constant ( $S^{\text{eff}}, r_p, \mu^{\text{stat}} = (0.05, 75, 20)$ ). The dimensionless tensile force  $T/\eta_0 u_p L$  is plotted as a function of strain for these systems in Fig. 11. Tensile force data were averaged over deformation intervals of  $\Delta\varepsilon \sim 0.02$ . Each set of symbols in Fig. 11 represents an average of two simulation runs.

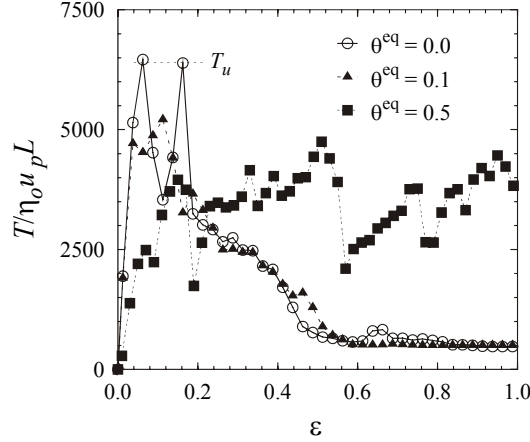


Figure 11. Dimensionless tensile force  $T/\eta_0 u_p L$  as a function of strain  $\varepsilon$  for networks of differently shaped fibers.

Features of the response are similar to that observed experimentally for the dry and rewet samples [9]. The tensile force initially varies linearly with deformation. The force then varies nonlinearly and passes through a maximum, accompanied with large fluctuations. The (average) rate of decrease of the tensile force after the maximum is smaller than the initial rate.

The fluctuations in tensile force correspond to fiber contacts breaking and reforming, analogous to that observed experimentally [9]. The tensile force increases as fibers align and deform; the tensile force decreases when contacts break (i.e., when the ratio of the friction force to the repulsive force at a contact exceeds  $\mu^{\text{stat}}$ ). The larger rapid decreases in the tensile force correspond to multiple contacts breaking virtually simultaneously. The fact that the fluctuations are rapid implies that the fibers are relatively stiff; when a contact breaks, fibers are able to spring back and reform new contacts very quickly relative to the rate of deformation.

The straight fiber network exhibits a rapid increase in tensile force as the sample is elongated, to a maximum value defined as the network tensile strength. Networks of slightly deformed fibers ( $\theta^{\text{eq}} = 0.1$ ) exhibit similar behavior, but with a smaller tensile strength. The tensile force for fiber networks with substantially deformed fibers ( $\theta^{\text{eq}} = 0.5$ ) increases more slowly with increasing deformation, and does not pass through a maximum over the deformation range simulated. The different responses for networks composed of straight and highly deformed fibers correspond to different structure evolutions. As illustrated in Fig. 10, networks of straight fibers develop a clear fracture zone at  $\varepsilon = 1.0$ . In contrast, networks of highly curved fibers exhibit incomplete fracture, with the network remaining partly intact to deformations  $\varepsilon > 1$ .

Simulations were performed using fibers of various lengths (aspect ratios  $r_p = 50, 75$ , and  $100$ ). The fibers were U-shaped and all had the same radius of curvature  $R_U = 59.5b$ . The radius of curvature is defined here as the average of the radii of circles tangent to the joints and segment centers,  $R_U = \ell [1/\sin(\theta^{\text{eq}}/2) + 1/\tan(\theta^{\text{eq}}/2)]/2$ . The effective stiffness  $S^{\text{eff}} = E_Y I / \eta_0 \gamma L^4$  was chosen to make the fiber stiffness ( $E_Y I$ ) constant [ $r_p = 50 \rightarrow S^{\text{eff}} = 0.25$ ;  $r_p = 75 \rightarrow S^{\text{eff}} = 0.05$ ;  $r_p = 100 \rightarrow S^{\text{eff}} = 0.016$ ]. All fibers interacted with the same coefficient of static friction,  $\mu^{\text{stat}} = 20$ .

The results for the dimensionless network force  $T/E_Y b^2$  as a function of strain are illustrated in Fig. 12. The network elastic modulus, defined as the initial slope of the tensile force as a function of strain, increases with increasing aspect ratio. The network strength increases and is shifted to larger deformations as the fiber aspect ratio is increased.

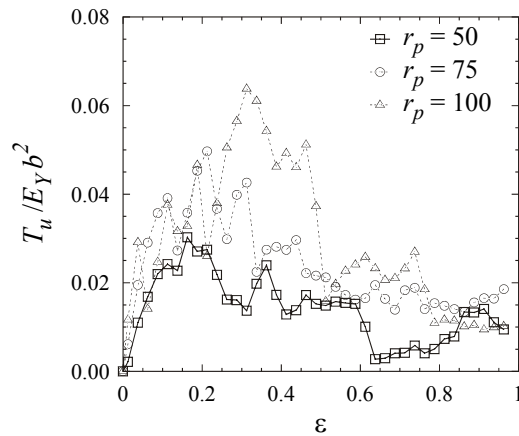


Figure 12. Dimensionless tensile force  $T/E_Y b^2$  as a function of strain  $\varepsilon$  for fibers of different aspect ratios.

These results are consistent with experimental results reported by Seth [22], who observed that the wet-web tensile strength of softwood pulp networks increased linearly with the average fiber length. This was attributed to longer fibers having an increased number of frictional contacts with other fibers. This is indeed observed in the simulations, where the average number of contacts per fiber (at  $\phi = 0.05$ ) are 2.5, 2.7 and 3.2 for the systems with fiber aspect ratios 50, 75 and 100, respectively.

## **CONCLUSION**

Fiber-level simulations examining flocculation in fiber suspensions, rheological properties, and handsheet formation and mechanical testing illustrate that such methods can be powerful tools for probing relationships between system variables, and understanding the mechanisms responsible for observed behavior. While simulations rely on models and thus should not be viewed as a replacement for experimental investigations, the ability to systematically examine effects of variables and phenomena make simulations useful for guiding experiments and reducing the number of experiments.

## **ACKNOWLEDGMENTS**

This project was supported in part by the National Research Initiative of the USDA Cooperative State Research, Education and Extension Service, grant number 2001-35103-09933.

## **REFERENCES**

1. Schmid, C. F., "Simulations of Flocculation in Flowing Fiber Suspensions," PhD thesis, University of Wisconsin-Madison (1999).
2. Schmid, C. F., and D. J. Klingenberg, "Mechanical flocculation in flowing fiber suspensions," *Phys. Rev. Lett.*, **84**, 290-293 (2000a).
3. Schmid, C. F., and D. J. Klingenberg, "Properties of fiber flocs with frictional and attractive interfiber forces," *J. Coll. Int. Sci.*, **226**, 136-144 (2000b).
4. Schmid, C. F., L. H. Switzer, and D. J. Klingenberg, "Simulations of fiber flocculation: Effects of fiber properties and interfiber friction," *J. Rheol.* **44**, 781-809 (2000).
5. Switzer III, L. H., "Simulating Systems of Flexible Fibers," PhD thesis, University of Wisconsin-Madison (2002).

6. Switzer III, L. H., and D. J. Klingenberg, "Rheology of sheared flexible fiber suspensions via fiber-level simulations," *J. Rheol.*, **47**, 759-778 (2003a).
7. Switzer III, L. H., and D. J. Klingenberg, "Simulations of fiber floc dispersion in linear flow fields," *Nordic Pulp Pap. Res. J.*, **18**, 141-144 (2003b).
8. Switzer III, L. H., and D. J. Klingenberg, "Flocculation in simulations of sheared fiber suspensions," *Int. J. Mult. Flow*, **30**, 67-87 (2004).
9. Switzer III, L. H., C. T. Scott, and D. J. Klingenberg, "Handsheets formation and mechanical testing via fiber-level simulations," *Nordic Pulp Pap. Res. J.*, **19**, 418-423 (2004).
10. Soszynski, R. M., and R. J. Kerekes, "Elastic interlocking of nylon fibers suspended in liquid. Part 1. Nature of cohesion among fibers," *Nordic J. Pulp Paper Res.*, **3**, 172-179 (1988).
11. Zhao, R. H., and R. J. Kerekes, "The effect of suspending liquid viscosity on fiber flocculation," *Tappi J.*, **76**, 183-188 (1993).
12. Zauscher, S., and D. J. Klingenberg, "Friction between cellulose surfaces measured with colloidal probe microscopy," *Coll. Surf. A*, **178**, 213-229 (2001a).
13. Amelina, E. A., E. D. Shchukin, A. M. Parfenova, A. I. Bessonov, and I. V. Videnskii, "Adhesion of cellulose fibers in liquid media: 1. Measurement of the contact friction force," *Coll. J.*, **60**, 537-540 (1998).
14. Sundararajakumar, R. R., and D. L. Koch, "Structure and properties of sheared fiber suspensions with mechanical contacts," *J. Non-Newton. Fluid Mech.*, **73**, 205-239 (1997).
15. Batchelor, G. K., "Slender-body theory for particles of arbitrary cross-section in Stokes flow," *J. Fluid Mech.* **44**, 419-440 (1970).
16. Petrich, M. P., D. L. Koch, and C. Cohen, "An experimental determination of the stress-microstructure relationship in semi-concentrated fiber suspensions," *J. Non-Newton. Fluid Mech.* **95**, 101-133 (2000).
17. Carrasco, B., and J. G. de la Torre, "Hydrodynamic properties of rigid particles: comparison of different modeling and computational procedures," *Biophysical J.*, **75**, 3044-3057 (1999).
18. Tozzi, E. J., C. T. Scott and D. J. Klingenberg, in preparation (2005).
19. Page, D. H., R. S. Seth, B. D. Jordan, M. C. Barbe, "Curl, crimps, kinks and microcompressions in pulp fibres: Their origin, measurement and significance," *Proc. 8th Fund. Res. Symp.: Fundamentals of papermaking*, Oxford UK, Volume 1, pages 183-227 (1985).
20. Kibblewhite R. P., and D. B. Brookes, "Factors which influence the wet web strength of commercial pulps," *Appita*, **8**, 227-231 (1975).
21. Miettinen, P., C. T. Scott, and D. J. Klingenberg, in preparation (2005).
22. Seth, R. S., "The effect of fiber length and coarseness on the tensile strength of wet webs: a statistical geometry explanation," *Tappi J.*, **78**, 99-102 (1995).

# Simulations of Flexible Fiber Suspensions



Emilio J. Tozzi and Daniel J. Klingenberg  
 Department of Chemical and Biological Engineering, and Rheology Research Center  
 University of Wisconsin, Madison, WI

C. Tim Scott  
 USDA Forest Products Lab, Madison, WI

Pasi Miettinen  
 KCL Science and Consulting, FIN-02151 Espoo, FINLAND

---

---

---

---

---

---

---

---

## Outline

- Flocculation behavior
  - Friction-induced flocculation
  - Influenced by length, flexibility, shape, interactions
- Rheology
  - Influenced by length, flexibility, shape, interactions
  - New shape measures
- Handsheet formation and testing
  - Influenced by length, flexibility, shape, interactions

---

---

---

---

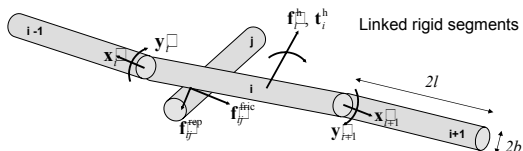
---

---

---

---

## Flexible Fiber Model



- hydrodynamic forces and torques
- bending and twisting stiffness  $S^{eff} = \frac{E_p I}{\eta_p \dot{\gamma} L^2}$
- inextensibility forces
- interparticle forces (excluded volume, friction, attraction)
- neglect Brownian motion, inertia and hydrodynamic interactions

Sundararajakumar and Koch. *J. Non-Newtonian Fluid Mech.* 73: 205, (1997)

---

---

---

---

---

---

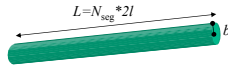
---

---

## Parameter Definitions

concentration –  $nL^3$

aspect ratio –  $r_p = L/2b$



coefficient of friction –  $\mu^{stat}, \mu^{kin}$

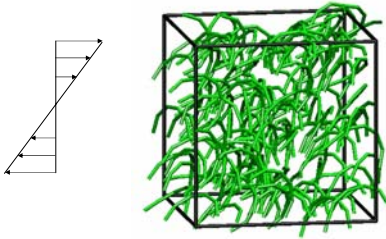
equilibrium shape –  $\theta^{eq}, \phi^{eq}$



flexibility –  $S^{eff} \equiv \frac{E_y I}{\eta_o \dot{\gamma} L^4}$

repulsion –  $\mathbf{F}_y^N = -F \exp[-ah_y] \mathbf{n}_y$

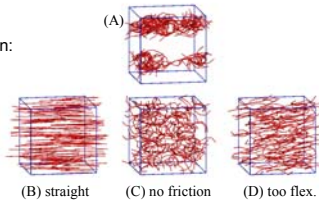
## Flocculation in Flowing Suspensions



## Flocculation Behavior

Factors that control flocculation:

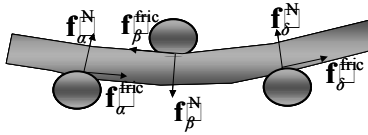
1. flexibility
2. equilibrium shape
3. interfiber friction



$$r_p = 75, \quad nL^3 = 20$$

|              |                   |                    |
|--------------|-------------------|--------------------|
| (A) helical  | $\mu^{stat} = 20$ | $S^{eff} = 0.05$   |
| (B) straight | $\mu^{stat} = 20$ | $S^{eff} = 0.05$   |
| (C) helical  | $\mu^{stat} = 0$  | $S^{eff} = 0.05$   |
| (D) helical  | $\mu^{stat} = 20$ | $S^{eff} = 0.0005$ |

## Elastic Fiber Interlocking



- Fibers are caught in elastically strained configurations
- Friction forces hold the network together

(Meyer and Wahren, *Svensk Papperstidn.*, 67, 432 (1964)  
 Soszynski and Kerekes, *Nordic Pulp Pap. Res. J.*, 3, 172 (1988))

---

---

---

---

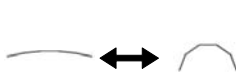
---

---

---

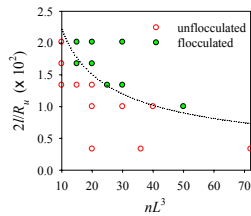
---

## Effect of Equilibrium Shape



Flocculation shifts to smaller concentrations with increasing fiber curvature

$$r_p = 75, S^{\text{eff}} = 0.05, \mu^{\text{stat}} = 20, \phi^{\text{eq}} = 0$$




---

---

---

---

---

---

---

---

## Suspension Rheology

- Bulk stress in a fiber suspension

$$\langle \boldsymbol{\sigma} \rangle = -p\boldsymbol{\delta} + 2\eta_o \mathbf{E}^{\infty} + \boldsymbol{\sigma}^p$$

- Approx.  $\boldsymbol{\sigma}^p$  using slender body theory

$$\boldsymbol{\sigma}^p = \frac{n}{2} \left\langle \int_{-\ell}^{\ell} [s\mathbf{p}\mathbf{F}(s) + \mathbf{F}(s)s\mathbf{p}] ds \right\rangle + \mathbf{F}^H \mathbf{r} + \bar{\mathbf{r}}\mathbf{F}^H + \Upsilon\boldsymbol{\delta}$$

---

---

---

---

---

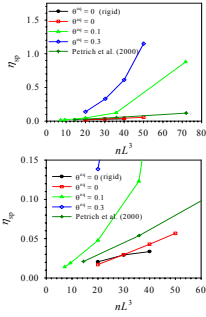
---

---

---

## Effect of Eqb. Shape on Viscosity

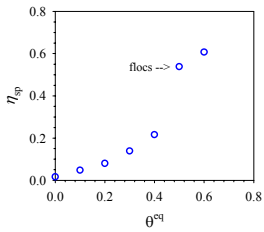
$S^{eff} = 0.05$ ,  $r_p = 75$ ,  $\phi^{eq} = 0$ ,  $\mu^{stat} = 20$



- Small permanent deformations – large effect
- Straight fibers – approx. by Batchelor's equation\*
 
$$\eta_{sp} \equiv \frac{\eta}{\eta_0} - 1 \propto nL^3$$
- Interactions are more important as fiber becomes more deformed

\*Batchelor. *J Fluid Mech.* 44, 1970.

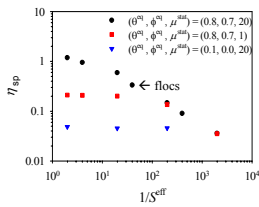
## Effect of Eqb. Shape on Viscosity



- As curvature increases, viscosity increases
- Large jump corresponds to flocculation

| $\theta^{eq}$ (rad) | shape |
|---------------------|-------|
| 0.0                 |       |
| 0.1                 |       |
| 0.3                 |       |
| 0.6                 |       |

## Rheology and Flocculation



- Shear thinning behavior shifted to lower shear rates
- Viscous forces dominate at high shear rates
- No "jump" in the stress as seen experimentally\*

\*Chen et al. *J. Soc. Rheol., Japan.* 30, 2002.

## Effect of Fiber Stiffness

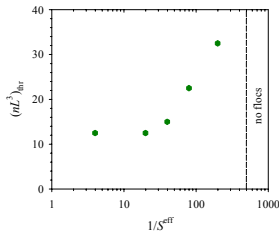
- Increasing  $S^{\text{eff}}$  => floccs at lower concentrations

$$\frac{1}{S^{\text{eff}}} \propto \eta_o$$

- Qualitative agreement with experiments\*

- As  $1/S^{\text{eff}}$  increases, viscous forces dominate

$$r_p = 75, \quad \mu^{\text{stat}} = 20, \quad \theta^{\text{eq}} = 0.6, \quad \phi^{\text{eq}} = 0$$



$$S^{\text{eff}} = \frac{E_y I}{\eta_o \dot{\gamma} L^4}$$

\*Soszynski and Kerekes. *Nordic Pulp Pap. Res. J.* 4 (1988).

## Why is $\mu^{\text{stat}}$ so large?

- $\mu^{\text{stat}}$  required to see flocculation very large
  - experimentally,  $\mu^{\text{stat}} \sim 0.5$

- Simulated fibers are not stiff enough

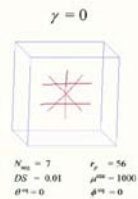
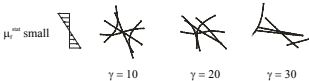
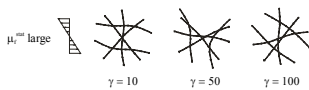
$$S^{\text{eff}} = \frac{E_y I}{\eta_o \dot{\gamma} L^4}$$

$10^{-1}$  (for  $S^{\text{eff}}$ ),  $10^{-3} \text{ Pa}\cdot\text{s}$  (for  $\eta_o$ ),  $10 \text{ s}^{-1}$  (for  $\dot{\gamma}$ ),  $10^{-3} \text{ m}$  (for  $L$ )  
 $E_y I = 10^{15} \text{ N}\cdot\text{m}^2$   
 $E_y I_{\text{exper.}} \approx 10^{12} \text{ N}\cdot\text{m}^2$

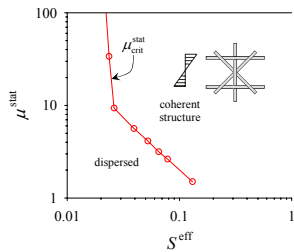
- Can flocculation occur for realistic  $\mu^{\text{stat}}$  if  $S^{\text{eff}}$  is more realistic?

\*Tam Doo and Kerekes. *Tappi J.* 64(3), 1983.

## $\mu_{\text{crit}}^{\text{stat}}$ vs $S^{\text{eff}}$ for a test floc



## $\mu_{crit}^{stat}$ vs $S^{eff}$ for a test floc



## Summary of Simulations

- Fiber shape affects
  - Flocculation behavior
  - Structure
  - Dynamics
  - Rheology
- Hydrodynamics important
  - Shape alters orbit dynamics
  - Changes frequency of collisions
  - Hydrodynamics in simulations sufficient?
- Shape Measures
  - How do you quantify "shape"?
  - Need to separate effects of shape from effects of flexibility, friction, concentration, etc.

## RPY Bead-Shell Model

- Model fiber as a shell composed of beads
- Intrafiber hydrodynamic interactions: Rotne-Prager-Yamakawa (RPY) tensor

$$\begin{bmatrix} \mathbf{u}_1^{\square} - \mathbf{U}_1^{\square} \\ \mathbf{u}_2^{\square} - \mathbf{U}_2^{\square} \\ \vdots \end{bmatrix} = \begin{bmatrix} \mathbf{T}_{11}^{\square} & \mathbf{T}_{12}^{\square} & \cdots \\ \mathbf{T}_{21}^{\square} & \mathbf{T}_{22}^{\square} & \cdots \\ \vdots & \vdots & \ddots \end{bmatrix} \begin{bmatrix} \mathbf{F}_1^{\square} \\ \mathbf{F}_2^{\square} \\ \vdots \end{bmatrix}$$

$$\mathbf{T}_{ij}^{\square} = \delta_{ij} \frac{1}{6\pi\mu a} \quad i = j$$

$$\mathbf{T}_{ij}^{\square} = \frac{1}{8\pi\mu r_{ij}} \left[ \delta_{ij} + \frac{\mathbf{r}_i \mathbf{r}_j}{r_{ij}^2} + \frac{2a^2}{r_{ij}^2} \left( \frac{1}{3} \delta_{ij} - \frac{\mathbf{r}_i \mathbf{r}_j}{r_{ij}^2} \right) \right] \quad i \neq j$$



## Resistance Matrix

$$\begin{bmatrix} \mathbf{F} \\ \mathbf{T} \\ \mathbf{S} \end{bmatrix} = \begin{bmatrix} \mathbf{A} & \tilde{\mathbf{B}} & \tilde{\mathbf{G}} \\ \mathbf{B} & \mathbf{C} & \tilde{\mathbf{H}} \\ \mathbf{G} & \mathbf{H} & \mathbf{M} \end{bmatrix} \begin{bmatrix} \mathbf{u}^{\infty} - \mathbf{U} \\ \boldsymbol{\omega}^{\infty} - \boldsymbol{\Omega} \\ \mathbf{E} \end{bmatrix}$$

Calculating  $\begin{bmatrix} \mathbf{F} \\ \mathbf{T} \\ \mathbf{S} \end{bmatrix}$  for various  $\begin{bmatrix} \mathbf{u}^{\infty} - \mathbf{U} \\ \boldsymbol{\omega}^{\infty} - \boldsymbol{\Omega} \\ \mathbf{E} \end{bmatrix}$  gives  $\begin{bmatrix} \mathbf{A} & \tilde{\mathbf{B}} & \tilde{\mathbf{G}} \\ \mathbf{B} & \mathbf{C} & \tilde{\mathbf{H}} \\ \mathbf{G} & \mathbf{H} & \mathbf{M} \end{bmatrix}$

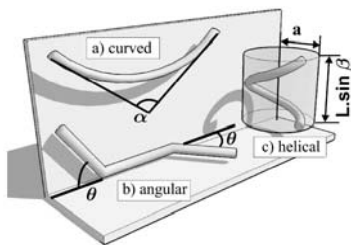
## Fiber Dynamics

$$\begin{bmatrix} \mathbf{u}^{\infty} - \mathbf{U} \\ \boldsymbol{\omega}^{\infty} - \boldsymbol{\Omega} \end{bmatrix} = \begin{bmatrix} -[\mathbf{A} & \tilde{\mathbf{B}}]^{-1} \\ \mathbf{B} & \mathbf{C} \end{bmatrix} \cdot [\tilde{\mathbf{G}} & \tilde{\mathbf{H}}] \cdot [\mathbf{E}]$$

$$[\mathbf{S}] = \begin{bmatrix} -[\mathbf{G} & \mathbf{H}] \\ \mathbf{A} & \tilde{\mathbf{B}} \\ \mathbf{B} & \mathbf{C} \end{bmatrix} \cdot [\tilde{\mathbf{G}} & \tilde{\mathbf{H}}] \cdot [\mathbf{M}] \cdot [\mathbf{E}]$$

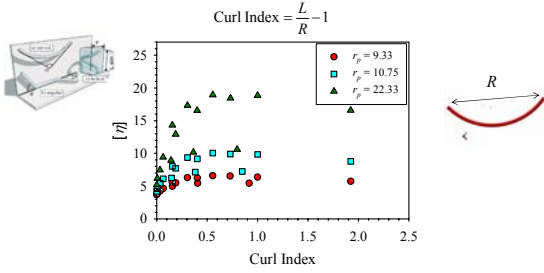
$$\boldsymbol{\sigma} = I \cdot \mathbf{T} + 2\mu \mathbf{E} + \frac{1}{V} \sum \mathbf{S}$$

## Different Fiber Shapes



- examine different measures of fiber shape and their correlation with rheological properties

## Correlation of Rheology with Shape



Page, D. H., R. S. Seth, B. D. Jordan, M. C. Barbe, Proc. 8th Fund. Res. Symp.: Fundamentals of Papermaking, Oxford UK, Volume 1, pages 183-227 (1985).

---

---

---

---

---

---

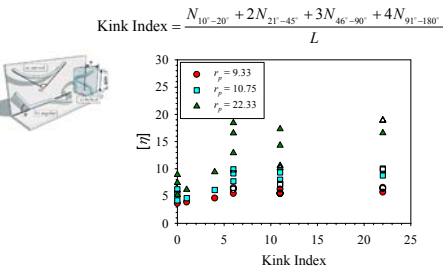
---

---

---

---

## Correlation of Rheology with Shape



Kibblewhite R. P., and D. B. Brookes, *Appita*, 8, 227-231 (1975).

---

---

---

---

---

---

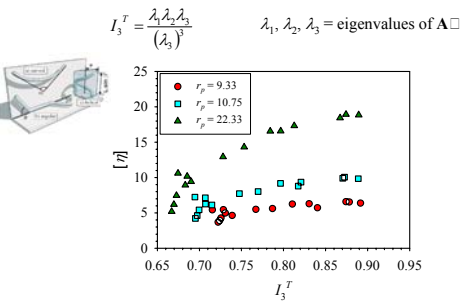
---

---

---

---

## Correlation of Rheology with Shape



Tozzi et al., in preparation

---

---

---

---

---

---

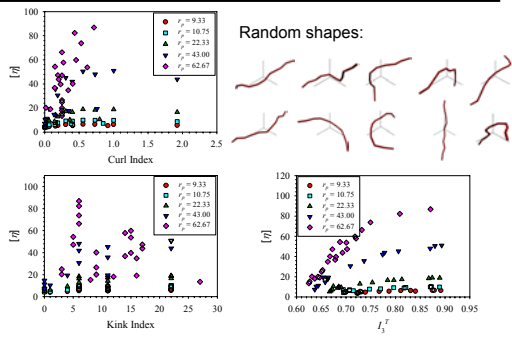
---

---

---

---

## Correlation of Rheology with Shape




---

---

---

---

---

---

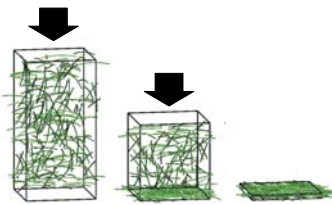
---

---

---

---

## Planar Fiber Networks



- Form a "handsheet" between surfaces
- Squeeze out suspending fluid

---

---

---

---

---

---

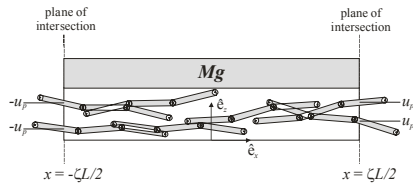
---

---

---

---

## Mechanical Testing




---

---

---

---

---

---

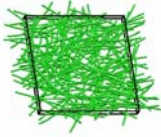
---

---

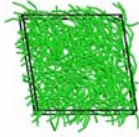
---

---

## Mechanical Testing



$r_p = 75$   
 $S^{\text{eff}} = 0.05$   
 $\theta^{\text{eq}} = 0.1$   
 $\phi^{\text{eq}} = 0$   
 $\mu^{\text{stat}} = 20$



$r_p = 75$   
 $S^{\text{eff}} = 0.05$   
 $\theta^{\text{eq}} = 0.6$   
 $\phi^{\text{eq}} = 0$   
 $\mu^{\text{stat}} = 20$

---

---

---

---

---

---

---

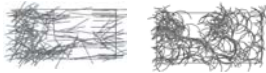
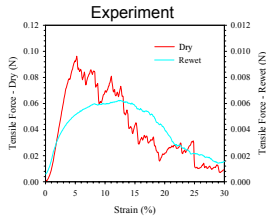
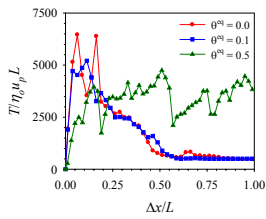
---

---

---

## Mechanical Response

$r_p = 75$ ,  $S^{\text{eff}} = 0.05$ ,  $\phi^{\text{eq}} = 0$ ,  $\mu^{\text{stat}} = 20$



Bleached softwood fibers, 10 g/m<sup>2</sup>, L = 2 mm

Switzer et al., Nordic Pulp Pap. Res. J., 19, 418 (2004).

---

---

---

---

---

---

---

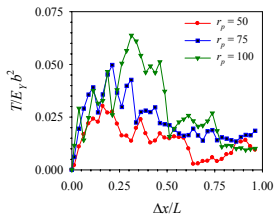
---

---

---

## Effect of Fiber Length

$R_{ij} = 29b$ ,  $\mu^{\text{stat}} = 20$ ,  $E_f I = \text{constant}$



- Increasing fiber length:
  - increases network strength
  - decreases network stiffness
- Consistent with experiments on wet-webs\*
  - $T \propto L$
  - increased frictional contacts

\*Seth. Tappi J. 78, 1995.

---

---

---

---

---

---

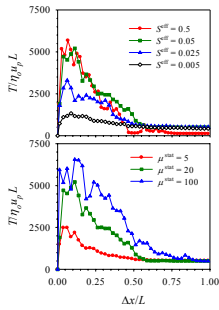
---

---

---

---

## Fiber Stiffness and Friction



$$r_p = 75, \quad \theta^{eq} = 0.1, \quad \phi^{eq} = 0$$

- Increasing  $S^{eff}$  or  $\mu^{stat}$  increases network strength
- Consistent with elastic fiber interlocking

---

---

---

---

---

---

---

---

---

---

## Conclusions

- Flocculation
  - Shape, flexibility, and friction are important
  - Elastic fiber interlocking holds fibers together
- Rheology
  - Fiber shape is important
  - Better measures than Curl & Kink indices
- Planar fiber networks
  - Strength depends on shape, flexibility, and friction
  - Compares qualitatively with experiments
- Value of simulations:
  - Understanding mechanisms
  - Systematic variation of parameters

---

---

---

---

---

---

---

---

---

---

## Acknowledgments

**People:** □

Russell Ross  
Paal Skjetne  
Heiko Bette

Chris Schmid  
Stefan Zauscher  
Len Switzer

**Funding:** □

USDA (NRICGP)  
USDA Forest Products Lab  
S. C. Johnson Foundation  
Norwegian Research Council

NSF  
Westvaco  
NATO  
TAPPI Foundation

---

---

---

---

---

---

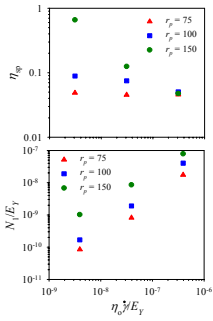
---

---

---

---

## Effect of Aspect Ratio



- Shear thinning more pronounced as  $r_p$  increases
- At large shear rates,  $\eta_{sp}$  appears independent of  $r_p$
- Results consistent with experiments<sup>‡</sup>

\*Goto et al., *Rheol. Acta*, 25, 1986.  
<sup>‡</sup>Kitano and Kataoka, *Rheol. Acta*, 20, 1981.

## RPY Bead-Shell Model

Total force on shell:  $\mathbf{F} \equiv \sum_i \mathbf{F}_i$

Total torque on shell:  $\mathbf{T} \equiv \sum_i \mathbf{r}_i \otimes \mathbf{F}_i$

Shell stresslet:  $\mathbf{S} \equiv \frac{1}{2} (\mathbf{D} \otimes \mathbf{D}^T) - \frac{1}{3} \delta \text{Tr}(\mathbf{D})$

$$\mathbf{D} \equiv \sum_i (\mathbf{F} \mathbf{r}_i)$$

Calculate  $\begin{bmatrix} \mathbf{F} \\ \mathbf{T} \\ \mathbf{S} \end{bmatrix}$  for various  $\begin{bmatrix} \mathbf{u}^{\infty} - \mathbf{U} \\ \boldsymbol{\omega}^{\infty} - \boldsymbol{\Omega} \\ \mathbf{E} \end{bmatrix}$



## Fiber Dynamics

$$\begin{bmatrix} \mathbf{u}^{\infty} - \mathbf{U} \\ \boldsymbol{\omega}^{\infty} - \boldsymbol{\Omega} \end{bmatrix} = \begin{bmatrix} \mathbf{A} & \tilde{\mathbf{B}} \\ \mathbf{B} & \mathbf{C} \end{bmatrix}^{-1} \cdot \begin{bmatrix} \tilde{\mathbf{G}} & \tilde{\mathbf{H}} \end{bmatrix} \cdot \mathbf{E}$$

Velocity and angular velocity of fiber

Constant matrix, function of shape.

Rate of strain

## Rheology

$$[\mathbf{S}] = -[\mathbf{G} \ \mathbf{H}] \begin{bmatrix} \mathbf{A} & \tilde{\mathbf{B}} \\ \mathbf{B} & \mathbf{C} \end{bmatrix}^{-1} \cdot [\tilde{\mathbf{G}} \ \tilde{\mathbf{H}}] \cdot [\mathbf{M}] \cdot [\mathbf{E}]$$

Stresslet  $\uparrow$   $\uparrow$  Rate of strain  $\uparrow$   
 Constant matrix, function of shape.

$$\boldsymbol{\sigma} = I.T. + 2\mu\mathbf{E} + \frac{1}{V} \sum \mathbf{S}$$

---

---

---

---

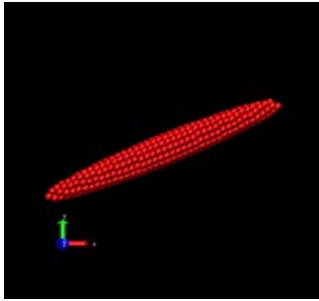
---

---

---

---

## Prolate Spheroid, $r_p = 10$




---

---

---

---

---

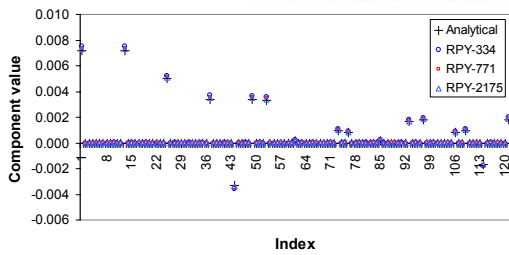
---

---

---

## Resistance Matrix Components

Prolate spheroid,  $r_p = 10$




---

---

---

---

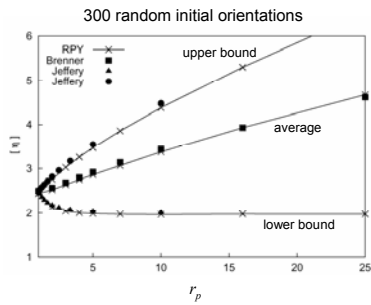
---

---

---

---

## Results for Spheroids



Jeffery, G. B., *Proc. Roy. Soc. Lond. A* **120**, 161 (1922).  
 Brenner, H., *Int. J. Multiphase Flow*, **1**, 195 (1974).

---

---

---

---

---

---

---

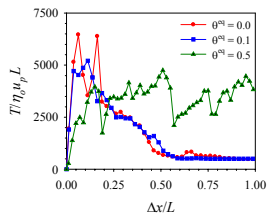
---

---

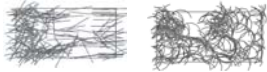
---

## Fiber Equilibrium Shape

$r_p = 75$ ,  $\Delta^{\text{eff}} = 0.05$ ,  $\phi^{\text{eq}} = 0$ ,  $\mu^{\text{stat}} = 20$



- Straighter fibers give larger tensile strengths
- Deformation increases the network flexibility




---

---

---

---

---

---

---

---

---

---

## Conclusions

- Fiber shape affects
  - Flocculation behavior
  - Structure
  - Dynamics
  - Rheology
- Shape measures
  - Curl index & kink index not as good
  - Invariants of  $A$  correlate better with  $[\eta]$

---

---

---

---

---

---

---

---

---

---

## Acknowledgments

**People:**

Russell Ross  
 Paal Skjetne  
 Heiko Bette

Chris Schmid  
 Stefan Zauscher  
 Len Switzer

**Funding:**

USDA (NRICGP)  
 USDA Forest Products Lab  
 S. C. Johnson Foundation  
 Norwegian Research Council

NSF  
 Westvaco  
 NATO  
 TAPPI Foundation

---

---

---

---

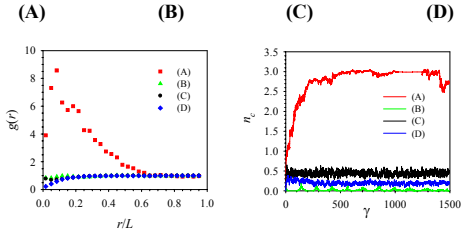
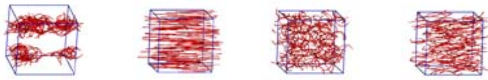
---

---

---

---

## Measuring Suspension Structure




---

---

---

---

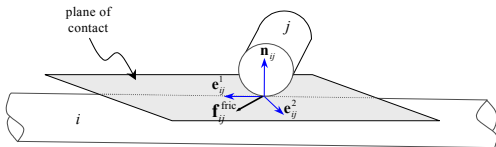
---

---

---

---

## Contact Forces



- Contact force decomposed into two contributions:
  - normal force – excluded volume and/or attractive
  - tangential force – static or kinetic friction

---

---

---

---

---

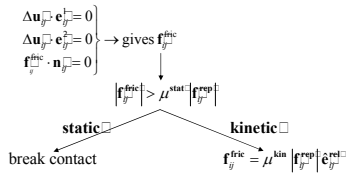
---

---

---

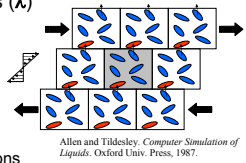
## Friction Constraint

- Constraint – no relative motion in the plane of contact
- Solve explicitly for the unknown friction forces
- Apply Coulombic friction law



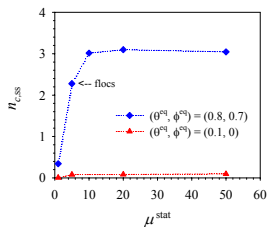
## Computational Algorithm

- System of differential algebraic equations (DAEs)
  - $\dot{\mathbf{q}} = \mathbf{F}(\mathbf{q}, \boldsymbol{\lambda}) = \mathbf{0}$  – equations of motion
  - $\Phi(\mathbf{q}) = \mathbf{0}$  – joint constraint
  - $\Psi(\mathbf{q}, \dot{\mathbf{q}}, \boldsymbol{\lambda}) = \mathbf{0}$  – friction constraint
- Approximate constraint forces ( $\boldsymbol{\lambda}$ )
- Periodic boundary conditions
  - $\rightarrow$  Lees-Edwards modification
- Integrate equations of motion
  - $\rightarrow$  updated positions and orientations

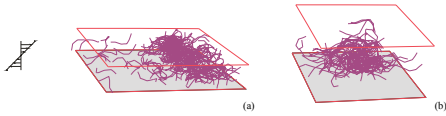


## Effect of $\mu^{stat}$

- as  $\mu^{stat}$  increases, heterogeneity increases
- for  $\mu^{stat} \geq \mu_{max}^{stat}$ , structure no longer changes



## Effects of Bounding Surfaces



gap =  $0.7 L$

gap =  $1.25 L$



Flocs formed by shearing a suspension in a small gap (gap = 1 mm; fiber length = 2 mm); long axis aligned with vorticity.

---

---

---

---

---

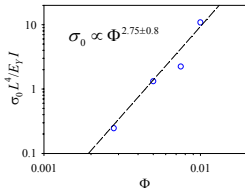
---

---

---

## Yield Stress of a Fiber Suspension

dynamic yield stress



- Network theory suggests

$$\sigma_0 \propto \Phi^3$$

- The model agrees with static yield stress measurements.\*
- Different dependence on fiber elastic modulus
  - surface effects
  - shape

\*Bennington et al., *Can. J. Chem. Eng.* 68, 1990.

---

---

---

---

---

---

---

---

## Dynamics

$$[\mathbf{S}] = [\mathbf{G} \quad \mathbf{H} \quad \mathbf{M}] \cdot \begin{bmatrix} \mathbf{u}^\infty - \mathbf{U} \\ \boldsymbol{\omega}^\infty - \boldsymbol{\Omega} \\ \mathbf{E} \end{bmatrix}$$

Stresslet Constant matrix, function of shape. Flow field

---

---

---

---

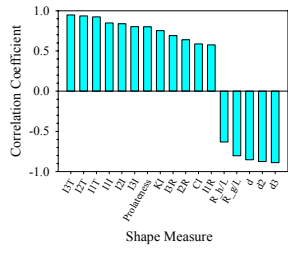
---

---

---

---

# Correlation of Rheology with Shape



---

---

---

---

---

---

---

---

In: Proceedings of the 2005 TAPPI practical papermaking conference. 2005 May 22-25; Milwaukee, WI. Atlanta, GA: TAPPI Press: Available: CD Rom-ISBN: 1-59510-094-6. Available online: <http://www.tappi.org>.